Controlling the Formation of Electroactive Graphene-Based Cementitious Composites: Towards Structural Health Monitoring of Civil Structures

Malgorzata Safuta, Artur Ciesielski, Paolo Samori

▶ **To cite this version:**

Malgorzata Safuta, Artur Ciesielski, Paolo Samori. Controlling the Formation of Electroactive Graphene-Based Cementitious Composites: Towards Structural Health Monitoring of Civil Structures. Chemistry - A European Journal, In press, 10.1002/chem.202301816 . hal-04240347

HAL Id: hal-04240347
https://hal.science/hal-04240347

Submitted on 13 Oct 2023

HAL is a multi-disciplinary open access archive for the deposit and dissemination of scientific research documents, whether they are published or not. The documents may come from teaching and research institutions in France or abroad, or from public or private research centers.

L'archive ouverte pluridisciplinaire **HAL**, est destinée au dépôt et à la diffusion de documents scientifiques de niveau recherche, publiés ou non, émanant des établissements d'enseignement et de recherche français ou étrangers, des laboratoires publics ou privés.

Check for updates

Chemistry
A European
Journal

Chemistry Europe
European Chemical Societies Publishing

Accepted Article

Title: Controlling the Formation of Electroactive Graphene-Based Cementitious Composites: Towards Structural Health Monitoring of Civil Structures

Authors: Małgorzata Safuta, Artur Ciesielski, and Paolo Samori

This manuscript has been accepted after peer review and appears as an Accepted Article online prior to editing, proofing, and formal publication of the final Version of Record (VoR). The VoR will be published online in Early View as soon as possible and may be different to this Accepted Article as a result of editing. Readers should obtain the VoR from the journal website shown below when it is published to ensure accuracy of information. The authors are responsible for the content of this Accepted Article.

To be cited as: *Chem. Eur. J.* **2023**, e202301816

Link to VoR: https://doi.org/10.1002/chem.202301816

WILEY VCH

10.1002/chem.202301816

15213765, ja, Downloaded from https://chemistry-europe.onlinelibrary.wiley.com/doi/10.1002/chem.202301816 by Cochrane France, Wiley Online Library on [13/10/2023]. See the Terms and Conditions (https://onlinelibrary.wiley.com/terms-and-conditions) on Wiley Online Library for rules of use; OA articles are governed by the applicable Creative Commons License

Accepted Manuscript

WILEY VCH

RESEARCH ARTICLE

Controlling the Formation of Electroactive Graphene-Based Cementitious Composites: Towards Structural Health Monitoring of Civil Structures

Małgorzata Safuta,*[a,b] Artur Ciesielski[a] and Paolo Samorì*[a]

[a] Dr. M. Safuta, Dr. A. Ciesielski, Prof. P. Samorì
Institut de Science et d'Ingénierie Supramoléculaires
Université de Strasbourg, CNRS
8 allée Gaspard Monge, 67000 Strasbourg (France)
E-mail: samori@unistra.fr

[b] Dr. M. Safuta
Department of Structural Engineering
Faculty of Civil Engineering
Silesian University of Technology
Akademicka 5, 44-100 Gliwice (Poland)
E-mail: malgorzata.safuta@polsl.pl

Supporting information for this article is given via a link at the end of the document.

Abstract: The development of composites combining multiple components each one imparting a specific function to the ensemble is highly sought after for disruptive applications in chemistry and materials science, with a particular importance for the realization of smart structures. Here we report on the development of an unprecedented multifunctional cementitious composite incorporating reduced graphene oxide (rGO). By design, this material features significantly enhanced electrical properties while retaining the excellent cement's hydration and microstructure. The multiscale investigation on the chemical and physical properties of the dispersion made it possible to establish an efficient preparation protocol for rGO aqueous dispersion as well as rGO-based cementitious composites using a commercial poly(carboxylate ether)-based superplasticizer. The conduction mechanisms within the matrix of rGO containing mortars were unraveled by electrochemical impedance spectroscopy revealing conductive paths originating from bulk cement matrix and rGO nanosheets in composites with rGO loadings as low as 0.075wt.%. For this rGO loading, we observed the reduction of the resistivity of bulk cement mortar layers from 18.3 MΩ cm to 2.8 MΩ cm. Moreover, the addition of 0.2 wt.% of rGO resulted in the formation of rGO conductive paths with the resistivity of 51.1 kΩ cm. These findings represent a major step forward towards the practical application of graphene-based materials in structural health monitoring of concrete structures.

Introduction

With the global consumption reaching 30 Gt per year,[1,2] concrete represents a fundamental component in most civil structures of our era: from residential buildings to water and wastewater systems, from power plants to transportation networks – concrete shapes our world. Almost 200 years after the development of Portland cement formula in 1824,[3] cement composites are still revolutionizing the construction industry - the consumption of concrete is now 3 times greater than 40 years ago,[2] and it is still growing exponentially due to the continued population growth and rapid urbanization. Despite the long list of advantages held by concrete, including fast-developing high compressive strength, low cost, excellent fire resistance and the ease of production,[4–6] which have paved the way towards a wide range of applications in civil engineering, the extensive use of concrete continues to raise public health and environmental concerns. Colossal carbon footprint,[2,7] high water consumption,[5] natural resources scarcity and potential health risks caused by greenhouse gas emission[8] – all that contributes to the negative society perception of concrete production. In light of this, minimizing the consumption of concrete components, and thus limiting its harmful environmental impact, by extending the service life of concrete structures and preventing them from premature degradation and failure are crucial goals from both economic and social perspective.

The structural integrity of concrete structures deteriorates over time due to the combination of various factors that may occur during the whole life cycle of concrete buildings, in particular (1) inadequate design and construction practices (calculation errors, inappropriate curing or workmanship), (2) improper maintenance (unforeseen vibrations, overloading of the structure and its improper use), and (3) chemical degradation due to exposure to harmful environmental and weather conditions (humidity, temperature changes, ingress of hazardous liquids and gases).[9–11] Therefore, frequent examination and monitoring of the technical conditions of structures are indispensable to ensure sustainable, reliable, safe and long-lasting concrete structures. For this reason, Structural Health Monitoring (SHM), *i.e.*, the continuous, real-time measurements and assessment of building

This article is protected by copyright. All rights reserved.

structures behavior, is becoming a widely employed structural diagnosis strategy.[10,12] Unlike the commonly used visual inspection, which remains extremely subjective, time-consuming and detects only damages visible to the human eye, thus on the surface and not in the bulk of the structure, SHM allows to identify and locate the structural cracks at the very initial stages of their formation as well as to monitor in real time stress, strain, deflections or even the weather conditions.[9,10,12] Typically, SHM is implemented in concrete structures through an external sensing, such as resistance strain gauges, fibre optic sensors, accelerometers, thermometers or piezoceramic transducers. Nevertheless, external sensing suffer from certain disadvantages that restrict its viable application in large-scale structures, such as insufficient compatibility with concrete structure, low durability, the need of extensive connections and equipment, high cost or, in case of embedded sensors, the interference in concrete structure.[11,12] Alternatively, self-sensing concrete, *i.e.*, concrete incorporating conductive functional fillers, holds potential to overcome the limitations of the external sensors enabling concrete to become a high-performance structural material integrating durable, multifunctional sensing capabilities by converting changes in the structure due to external stimuli into electrical response.[11,13] The understanding of the conduction mechanism is the foundation of controlling the self-sensing behavior of concrete. Basically, the saturated cement composites feature high conductivity due to the ionic conduction phenomenon. The movement of the ions within cement matrix leads to the electric polarization and makes the resistivity measurements highly sensitive to the changes of the environmental conditions or aging of the composites. Noteworthy, the incorporation of functional fillers into concrete gives an origin to additional conduction mechanisms, *i.e.*, tunneling, field emission and/or contact conduction. When the filler content highly exceeds the percolation threshold, that is the minimum loading of a filler, which will enable the formation of a conductive path within the composite, the filler particles contact each other and the contact conduction prevail over the other types of conduction, thus making the resistivity measurements independent from the moisture content or environmental conditions.[14] From this perspective, the choice of the functional filler is crucial for tailoring the properties of self-sensing concrete, since it dominates the sensing mechanism within cement matrix. Up to date, the most studied conductive fillers for self-sensing cement composites are carbon fibers and nanofibers, steel fibers, nickel powder, carbon black and graphite as well as carbon nanotubes.[13,15] Nevertheless, although the effectiveness of the abovementioned fillers has been comprehensively studied,[15,16] the design of the composition of self-sensing concrete remains a challenging and highly complex task. The electrical properties and sensing ability of cementitious composites depend on many factors and parameters of functional filler, in particular its chemical composition, morphology (shape, size, length, aspect ratio etc.) and concentration level as well as the quality of the dispersion of the filler within cement matrix.[15] Moreover, in view of the relatively high costs of the functional fillers, if compared with plain concrete, new types of conductive fillers allowing the development of self-sensing cementitious composites with low filler content are essential for the future technological applications of smart concrete.

After almost two decades of research on concrete nanotechnology, graphene – a 2D honeycomb lattice of sp^2 carbon atoms[17,18] – is still one of the most promising low dimensional materials for civil engineering applications. Although graphene has emerged as an exciting material holding numerous outstanding properties, in particular electrical ones, its application as a conductive filler in self-sensing concrete remains relatively unexplored. Initially, graphene oxide (GO) has become the focus and frontier of concrete nanotechnology due to its low-cost production and high dispersibility in water. The high dispersibility of GO in water originates from the oxygen functional groups: hydroxyl and epoxy groups located on the basal plane as well as carbonyl and carboxyl groups on the edges of GO nanosheets.[18] Although these functional groups may be greatly beneficial in GO-based composites serving as reactive sites and nucleation points for cement hydrates, they contribute as well to the formation of in plane defects and disorders within the electronic structure, thus making GO electrically insulating. However, the process of GO reduction offers the possibility to partially restore the conductivity of graphene due to the removal of oxygen atoms.[20,21] Chemical and thermal processes commonly adopted for the synthesis of reduced graphene oxide (rGO) allow the production of material with film resistance in the range of 10^{-3}-10^{-4} Ω m[20,22] and 10^{-2}-10^{-4} Ω m,[23,24] respectively. Although as produced rGO still possesses some intrinsic and extrinsic defects, the high yield, scalability, and low cost of GO reduction make it a prime candidate for developing self-sensing cementitious composites.[21]

Another common issue in the research on self-sensing concrete is the development of the relatively simple, precise and time efficient measurement method for determining the electrical properties of cement composites. In particular, the main crucial parameter to be considered is the type of applied current, *i.e.*, either direct current (DC) or alternating current (AC). While the measurements with the use of DC are clearly more straightforward, DC current will cause the movement and aggregation of the ions present in concrete pores and thus will lead to the electrical polarization. To circumvent this problem, the time of applying current should be extended as much as necessary to stabilize the measured resistivity. However, the polarization effect is strongly dependent on the specimen size and geometry, with large elements requiring more time to fully polarized, hence this method is technologically difficult and does not target real-scale applications.[15,25] On the contrary, the AC methods enables to attain an exquisite control over the polarization effect and the parameters measured using AC are much more stable. In particular, Electrochemical Impedance Spectroscopy (EIS) has become a widely employed powerful tool for non-destructive measurements of cement composites properties. Initially, EIS was mainly used to monitor the corrosion of concrete reinforcement, on-going hydration and microstructure of cement composites, carbonation processes and chloride migration.[26] More recently, EIS has emerged also as a powerful technique for the investigation of cement composites incorporating conductive additives allowing to gain detailed

This article is protected by copyright. All rights reserved.

15213765, ja, Downloaded from https://chemistry-europe.onlinelibrary.wiley.com/doi/10.1002/chem.202301816 by Cochrane France, Wiley Online Library on [13/10/2023]. See the Terms and Conditions (https://onlinelibrary.wiley.com/terms-and-conditions) on Wiley Online Library for rules of use; OA articles are governed by the applicable Creative Commons License

Accepted Manuscript

10.1002/chem.202301816

insight into the conduction mechanism and the quality of the functional filler dispersion.[27,28] Nevertheless, the high complexity of concrete microstructure as well as the lack of clear guidelines and well-established universal equivalent circuit for the fitting procedure makes it extremely challenging to fully interpret the results of impedance studies of cement composites. Therefore, further research in this field is essential to successfully apply electrochemical impedance spectroscopy in SHM.

Here we present an unprecedented cementitious composite incorporating rGO nanosheets. We first investigated the influence of different surfactants on the quality of rGO aqueous dispersion. The use of commercial poly(carboxylate ether)-based superplasticizer with rGO-to-surfactant ratio of 1:2 allowed us to obtain a homogenous and stable dispersion of rGO in water. Significantly, the consistency of fresh cement mortars as well as the cement hydration process and the microstructure of hardened composites remained unhampered, even with the rGO loading as high as 0.2 wt.%. We then performed the comprehensive electrochemical impedance spectroscopy measurements of hardened cement mortars at various saturation degrees. Based on models reported in the literature, we developed a new, modified equivalent electrical circuit mimicking the electrical response of both reference and rGO-based cement composites, allowing us to gain an insight into the conduction mechanisms within their microstructure. We noticed a significant change in the shape of Nyquist plot for composites containing low rGO loadings, indicating the formation of tunneling conduction rGO-based paths within cement matrix. These findings represent an important step forward for the practical application of graphene-family materials in multifunctional cement composites.

Results and Discussion

Reduction of GO

rGO has been prepared by the chemical reduction of graphene oxide using sodium hydrosulfite as the reducing agent (**Figure 1a**).[29] Noteworthy, chemical reduction was proved to be one of the most common and efficient methods for GO reduction. Although different compounds may be used as reducing agents in a process of chemical reduction of GO, such as hydrazine, hydroiodic acid or sodium borohydride,[23,29] their application is limited due to their toxicity, high cost, limited efficiency or additional undesirable functionalization of the resulting material. Alternatively, the use of sodium hydrosulfite allows to obtain non-functionalized rGO in a relatively straightforward and safe solution. Significantly, this process is highly scalable,[21] thus it holds a great technological potential for concrete applications. The reduction process lasting 20 h at 90°C allowed us to produce ca. 150 mg of dried rGO.

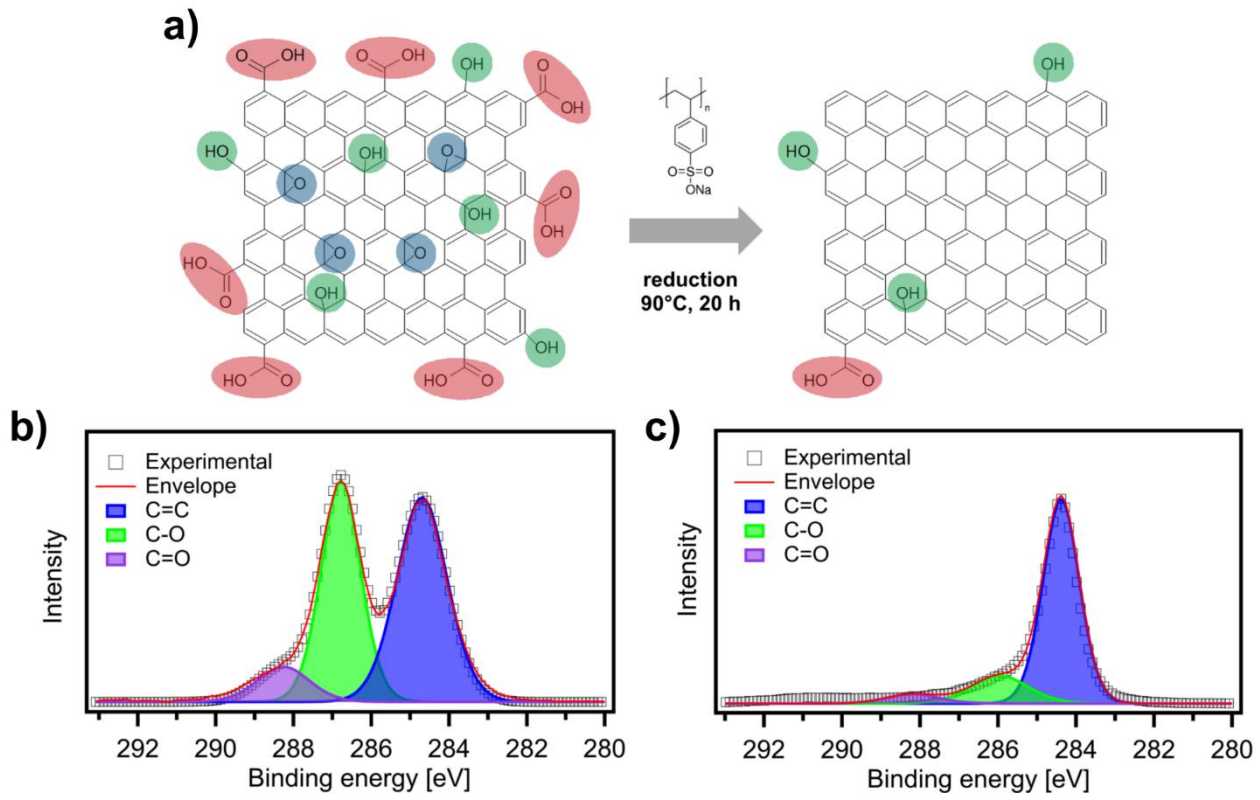

Figure 1. a) Chemical reduction of graphene oxide using sodium hydrosulfite. b) and c) Fitted XPS C 1s spectra of b) graphene oxide and c) reduced graphene oxide.

This article is protected by copyright. All rights reserved.

15213765, ja, Downloaded from https://chemistry-europe.onlinelibrary.wiley.com/doi/10.1002/chem.202301816 by Cochrane France, Wiley Online Library on [13/10/2023]. See the Terms and Conditions (https://onlinelibrary.wiley.com/terms-and-conditions) on Wiley Online Library for rules of use; OA articles are governed by the applicable Creative Commons License

Accepted Manuscript

10.1002/chem.202301816

The chemical composition and the oxidation degree of as prepared rGO were unraveled by X-ray photoelectron spectroscopy (XPS) and compared with the starting material, *i.e.*, graphene oxide. The analysis was performed to evaluate the efficiency of the reduction process by following the changes in oxygen functional groups in both materials. Figures 1b and c show the comparison of high-resolution C 1s spectra of GO and rGO. The spectra reveal the presence of an asymmetric C-C peak observed at 284.4 eV as well as two peaks attributed to the oxygen-containing groups, *i.e.*, C-O at 286-286.6 eV and C=O at 288.3 eV.[23] The oxidation degree of purchased GO is estimated for 41-50%, while ca. 12-14% of oxygen is present in rGO.

To cast further light onto the reduction process, we then performed conductivity measurements of rGO thin films with a four-point probe. Noteworthy, our attempts to characterize the sheet resistivity of GO films failed due to exciding the measurement range of the instrument (*i.e.*, 10^7 Ω sq^{-1}), while the resistivity of rGO films was in the range of 3.5-7*10^{-3} Ω m, thus confirming that the electrical properties were partially restored upon reducing the GO.

Dispersion of rGO in cement composites

The homogeneous dispersion of the functional filler within the cementitious matrix represents one among the main factors determining the electrical properties of self-sensing concrete. Nonuniformly dispersed filler may lead to the disrupted microstructure of cementitious composites resulting in decreased mechanical strength or durability. This issue is particularly relevant when dealing with two-dimensional materials: due to their hydrophobic nature and strong van der Waals forces, they unavoidably have a strong propensity to agglomerate and flocculate in water and/or cement environment.[30] Indeed, during the ongoing process of GO reduction, rGO becomes hydrophobic and its nanosheets start to aggregate due to the removal of oxygen atoms, thus making the preparation of rGO-based cement composites even more challenging.[20,29] Moreover, cementitious composites proved to be a hostile environment even for highly-dispersible graphene oxide due to their high alkalinity and presence of various ions, including Ca^{2+}, Na^{+}, K^{+}, OH^{-} and $(SO_4)^{2-}$.[3] In particular, several studies[31,32] showed that chemical cross-linking of GO nanosheets with calcium ions may lead to the immediate GO flocculation and formation of agglomerates.

Therefore, we opted first to investigate the stability of rGO aqueous dispersion in cement alkaline environment. Towards this end, we added 100 µl of solution extracted from fresh cement paste to 3.0 ml of aqueous dispersion of GO and rGO with concentration of 0.05 mg/ml. The addition of the solution has resulted in rapid and notable flocculation of GO, conversely not affecting rGO dispersions (see Figure S2a). These results can be ascribed, to a great extent, to the reduction process and thus to the removal of oxygen groups responsible for the formation of metal complexes with calcium ions. In order to get further insight into the mechanisms governing the efficiency of rGO dispersion within cement composites, we decided to introduce different amounts of cement grains into GO and rGO aqueous dispersions with the same concentration and volume, *i.e.*, 3 ml of dispersion with the concentration of 0.05 mg/ml. As shown in Figure S2b and c, the segregation of both GO and rGO is highly visible after the addition of cement. Both nanomaterials precipitate together with adsorbed cement particles to the bottom of the vial leaving the supernatant solution transparent. Even though the precipitation of GO is more rapid, if compared with rGO, the remaining oxygen groups still lead to the slow segregation of rGO with the addition of 8 mg of cement. Therefore, one can expect that the aqueous rGO dispersion will not remain stable while preparing rGO-based cement composites and thus the effective dispersing protocol needs to be first established.

Towards this aim, we evaluated the quality of rGO water dispersion prepared with five surfactants chosen due to their low cost and accessibility from those the most commonly adopted so far to disperse graphene-family materials in cement composites,[30] *i.e.*, poly(sodium 4-styrenesulfonate) (PSS), sodium dodecylbenzenesulfonate (SDBS), trimethyloctadecylammonium bromide (TODA) and two commercially available poly(carboxylate ether)-based (PCE) superplasticizers 6681F and 4930F (from BASF). All rGO suspensions were prepared with the surfactant-to-rGO ratio of 1 and concentration of 0.1 mg/ml by 30 min sonication in an ultrasonic bath. The quality of rGO dispersion is revealed in the UV-vis absorption spectra by the characteristic peak at ca. 270 nm of the wavelength (**Figure 2a**) with the higher absorbance indicating more homogenous dispersion. The quality of rGO control solution, *i.e.*, rGO water dispersion without any surfactant, turned out to be extremely low with the absorbance of ca. 0.093, while the addition of PCE superplasticizers allowed to achieve more homogenous rGO dispersions with the absorbance of 0.266 and 0.460 for 4930F and 6681F superplasticizers, respectively. On the contrary, the effect of SDBS and TODA on the dispersibility of rGO was negligible as evidenced by a minor increase in the absorbance from to 0.113 and 0.130, respectively. Moreover, the stability of rGO suspensions was assessed visually immediately after the sonication (Figure 2d) and 6 h later (Figure 2e). Noteworthy, the observations are in line with the UV-vis results. On one hand, the segregation of rGO in TODA and SDBS dispersions is highly visible with the naked eye, even immediately after the sonication. On the other hand, rGO dispersions prepared with the use of PCE superplasticizers and PSS featured the proper homogeneity. Significantly, the dispersion containing PCE 6681F was the only one that proved to be stable not only 6 h after the sonication, but also after a few days. Interestingly, the PCE superplasticizers play a double role in preventing rGO aggregation by the steric hindrance effect and electrostatic repulsion.[33] While the former allows to separate rGO nanosheets from charged ions, the latter prevents them for aggregating with each other.

Based on these results, we then aimed to establish the most advantageous surfactant-to-rGO ratio for 6681F superplasticizer. We found that the highest quality of rGO dispersion could be achieved for 1:1 and 1:2 surfactant-to-rGO ratio (Figure 2f and b). With the higher amount of PCE, the absorbance peak significantly decreases and rGO precipitates easily to the bottom of the tube. Since the quality of the dispersion can be also tuned by playing with sonication time, we then decided to explore the effect of various sonication time on the stability of rGO dispersion.

This article is protected by copyright. All rights reserved.

15213765, ja, Downloaded from https://chemistry-europe.onlinelibrary.wiley.com/doi/10.1002/chem.202301816 by Cochrane France, Wiley Online Library on [13/10/2023]. See the Terms and Conditions (https://onlinelibrary.wiley.com/terms-and-conditions) on Wiley Online Library for rules of use; OA articles are governed by the applicable Creative Commons License

Accepted Manuscript

10.1002/chem.202301816

Surprisingly, the sonication time turned out not to affect the dispersion quality significantly with the absorbance varying between 0.190 and 0.210.

Noteworthy, our observations are in line with previous studies reporting the high-quality rGO aqueous dispersion obtained with the use of PCE superplasticizers and sonication.[33,35,36] Even though the most favorable PCE-to-rGO ratio varies significantly among different reports, it should be highlighted that rGO dispersion ability may be also influenced by its possible functionalization during the synthesis and thus these values cannot be directly compared with each other.

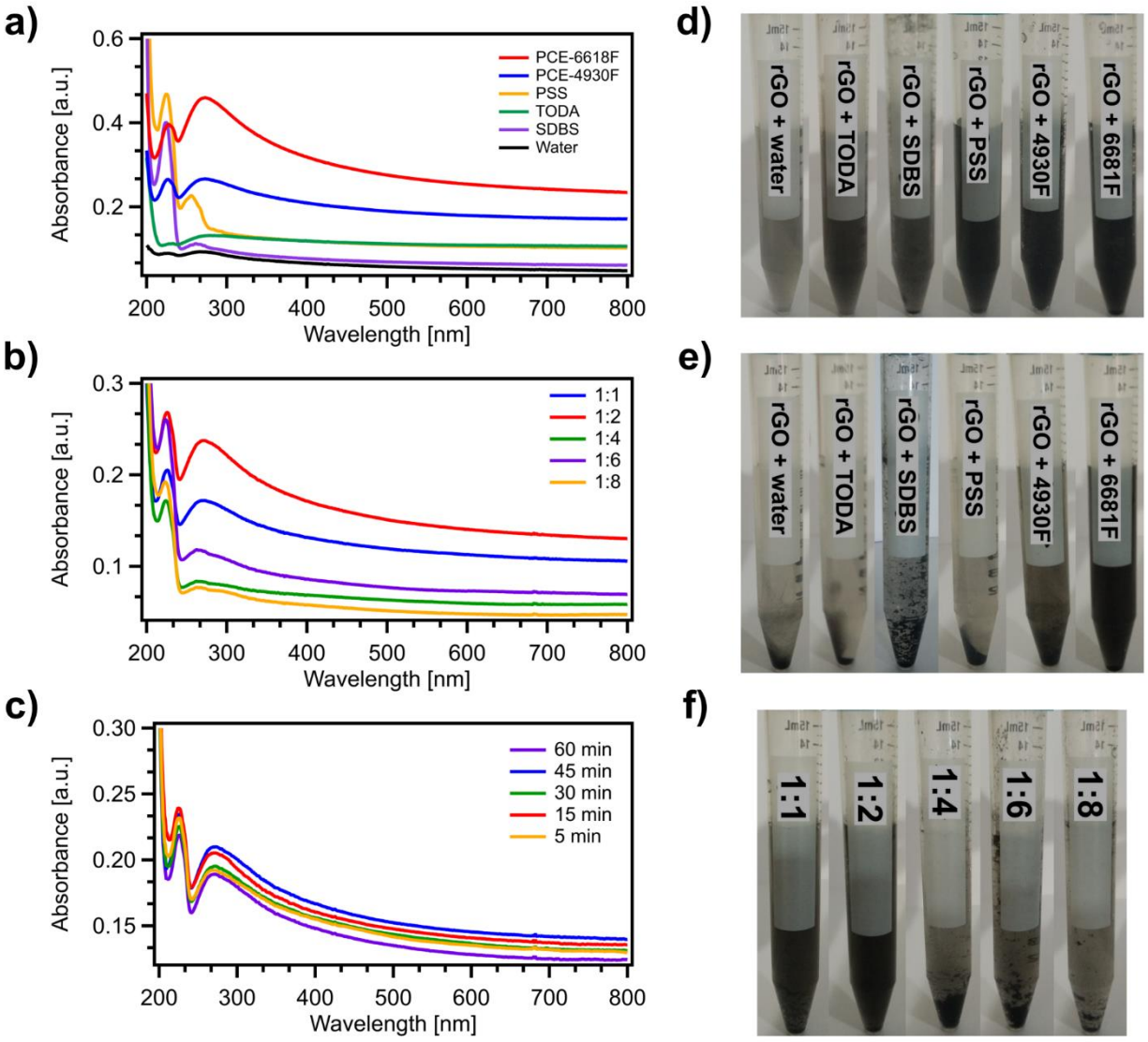

Figure 2. a), b) and c) UV-vis spectra of rGO aqueous solutions: a) with different surfactants, b) with various content of 6681F PCE and c) with 6681F PCE-to-rGO ratio of 2 after different sonication time. d) and e) Water dispersion of rGO with various surfactants: d) immediately after the sonication and e) after 6 h. f) Water dispersion of rGO with different content of 6618F PCE 6 h after the sonication.[34]

Electrochemical Impedance Spectroscopy

In order to determine the effect of rGO nanosheets on the electrical properties and conduction mechanism of cementitious composites, we then performed the comprehensive electrochemical impedance spectroscopy studies of hardened rGO-based cement mortars at different moisture content. We manufactured 13 cement mortars made out of Portland cement type I: two plain cement mortars with water-to-cement ratio of 0.5 and 0.45, cement mortars incorporating various loadings of rGO within the range of 0.025 wt.% up to 0.2 wt.% (added as rGO-PCE aqueous dispersion with rGO dosage by weight of cement) as well as mortars with the corresponding amounts of PCE. The labelling

This article is protected by copyright. All rights reserved.

15213765, ja, Downloaded from https://chemistry-europe.onlinelibrary.wiley.com/doi/10.1002/chem.202301816 by Cochrane France, Wiley Online Library on [13/10/2023]. See the Terms and Conditions (https://onlinelibrary.wiley.com/terms-and-conditions) on Wiley Online Library for rules of use; OA articles are governed by the applicable Creative Commons License

Accepted Manuscript

10.1002/chem.202301816

and exact composition of all composites are presented in Table S2 while the results of consistency measurements of fresh cement mortars may be found in Figure S3.

Noteworthy, the development of an efficient, time-effective and technologically simple protocol for the measurements of the electrical properties of cement composites represents one of the greatest challenges to be faced in the field of self-sensing concrete due to the high complexity of its microstructure combining different solid and liquid components. Intuitively, plain concrete in the dry state is considered as an electrically insulating material with the electrical resistivity of ca. 10^6-10^7 Ω cm.[37,38] On the other hand, with the increasing moisture content, cement composites become electrically conductive due to the ionic conduction phenomena depending strongly on the movement of ions in the interconnected pore network of hardened matrix.[27,39] Moreover, the scenario becomes even more complicated with the addition of conductive functional fillers – the electrical behavior of cement composites is then driven by a variety of conduction mechanisms, *i.e.*, ionic, tunneling and contact conduction.[16] In this perspective, Electrochemical Impedance Spectroscopy has emerged as a powerful tool allowing to distinguish between the conduction paths within concrete microstructure and to specify their contribution to the general electrical response of cement composites.[27]

Fundamentally, the impedance spectra are fitted with the equivalent electrical circuit being a set of electrical components, *e.g.*, resistors and capacitors, with a precise physical meaning and thus mimicking the microstructure and behavior of cement composites.[39,40] Nevertheless, the high complexity and heterogeneous nature preclude mostly the use of one universal equivalent circuit for all cement composites and therefore a plethora of different circuits have been proposed by researchers over the years.[41]

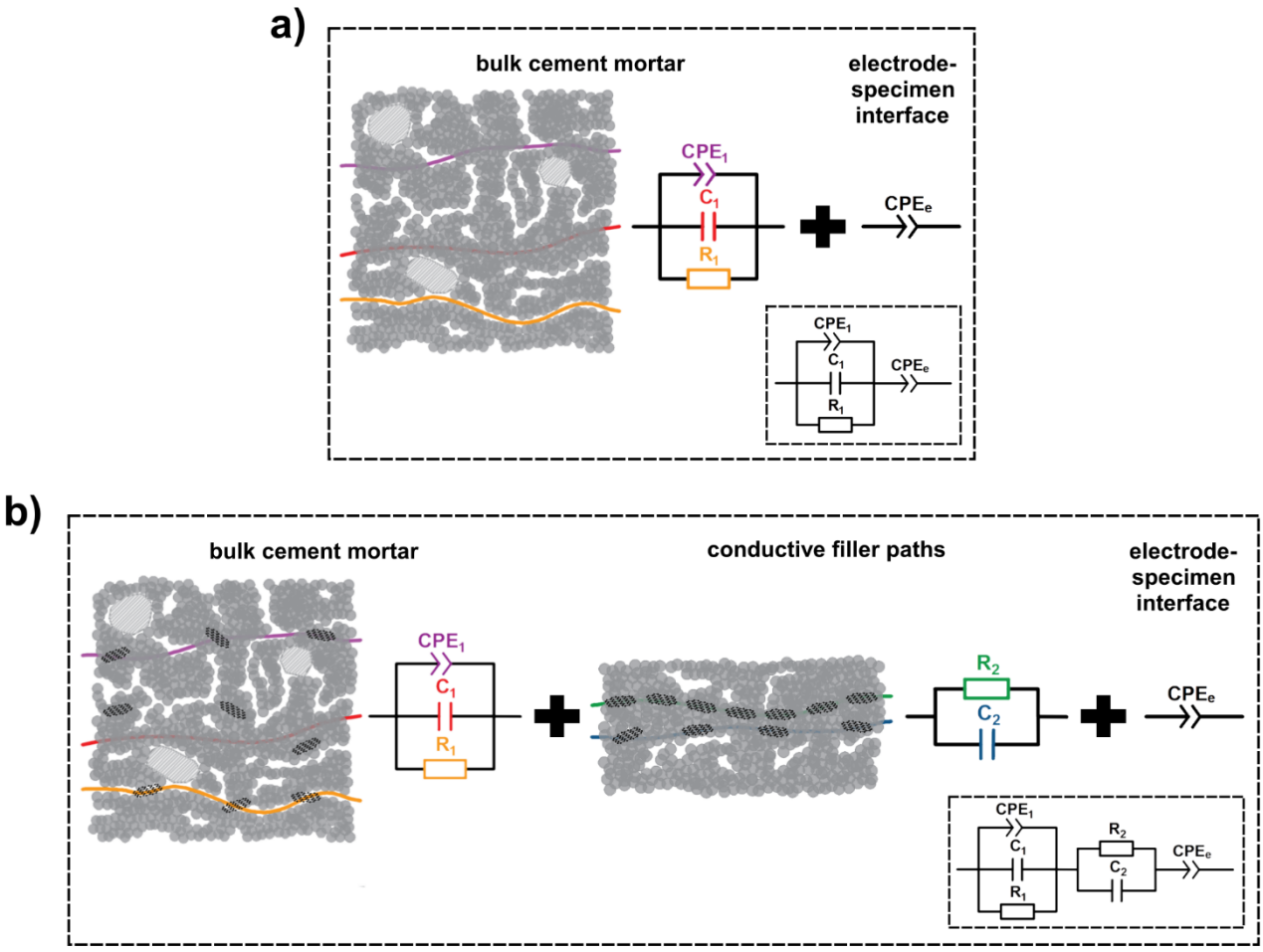

Figure 3. Equivalent electrical circuits applied for the fitting of impedance spectroscopy results of: a) plain cement mortars and b) cement mortars incorporating rGO (description in the text).

In order to further develop the universal equivalent circuit for rGO-based cementitious composites providing insight into the origin of their electrical response, we first focused our attention on the impedance spectroscopy analysis of reference cement mortar M1_R after applying different drying conditions: the hardened samples were first dried in the air for 7 days at ca. 20°C, followed

This article is protected by copyright. All rights reserved.

15213765, ja, Downloaded from https://chemistry-europe.onlinelibrary.wiley.com/doi/10.1002/chem.202301816 by Cochrane France, Wiley Online Library on [13/10/2023]. See the Terms and Conditions (https://onlinelibrary.wiley.com/terms-and-conditions) on Wiley Online Library for rules of use; OA articles are governed by the applicable Creative Commons License

Accepted Manuscript

10.1002/chem.202301816

by 5 days of oven drying at 60°C. Additional measurement was performed as well after 2 days of oven-drying. The impedance analysis was conducted with the signal amplitude of 0.3 V RMS and the frequency range between 0.1 Hz and 500 kHz. The EIS plots were then processed with the fitting procedure using the most common equivalent circuits reported in the literature, in particular the simplified equivalent circuit[39,42] consisting of two resistor-capacitor circuits corresponding to bulk cement matrix and the electrode-specimen interface as well as Song's circuit[41] with its further modification[43] involving the simulation of three conductive paths within cement composite connected in parallel, *i.e.*, continuous conductive paths (CCP, modelled by a resistor) of continuously connected micro-pores, insulator paths (IP, modelled by a capacitor) of the continuous solid phase of cement hydrates and mixed discontinuous conductive paths (DCP, modelled by a resistor and a capacitor connected in series).

To our surprise, the application of neither the simplified circuit nor the "conductive paths" circuit developed by Song[42] allowed us to achieve high compliance with the experimental results. While the former failed to accurately represent the shape of measured Nyquist plots due to being oversimplified, the latter generated high fitting errors in some spectra, in particular within the discontinuous conductive path indicating that the value of R_{DCP} approaches zero. Therefore, to overcome these limitations, we have developed a modified "conductive paths" circuit presented in **Figure 3a**. Although the representation of the impedance of the continuous conductive paths as well as the insulator paths remained unaltered, if compared to original circuit (resistor R_1 and capacitor C_1, respectively), we simulated the impedance of the discontinuous conductive paths as a single constant phase element CPE_1. Depending on the distribution of micro-pores and cement paste layers along the DCPs, the CPE_1 parameters will be closer to or further from an ideal capacitor behavior. Moreover, the electrode-specimen interface was modelled simply by introducing into the circuit a constant phase element CPE_e. Nevertheless, since this study is focused on the electrical response of bulk cement mortar with or without the addition of rGO, rather than on the electrode effect, the values of CPE_e were neglected in further discussion of the results. Noteworthy, all the measured spectra tend to intersect the origin of the Nyquist plot and no offset resistance was recorded. Therefore, the total impedance value for the equivalent circuit revealed in Figure 3a may be calculated as follows:

$$Z_A = \frac{1}{\frac{1}{R_1}+Q_1(j\omega)^{\alpha_1}+j\omega C_1} + \frac{1}{Q_e(j\omega)^{\alpha_e}} \quad (1)$$

where: Q_1, α_1, Q_e and α_e are the Q-factors and α-exponents of CPE_1 and CPE_e, respectively.

Figures 4a-c show the Nyquist plots for reference mortar M1_R after different drying conditions along with the fitting curves and the recorded values of the circuit components. Roughly speaking, the ongoing drying process results in a significant change of the impedance spectrum shape: when the constant frequency range is applied in all measurements, the high frequency arc becomes more visible, and the low frequency line starts to disappear together with the drying of the samples. Noteworthy, due to the evaporation of water from the pore system of cement mortar, the spectra are shifted along the real axis revealing the average change of the R_1 resistivity of CCPs from 40.5 kΩ cm for samples dried in the air for 7 days to 624.3 kΩ cm and 18.4 MΩ cm for samples dried in the oven for 2 and 5 days, respectively. Similar trend can be observed for the total impedance values (Figure 4d-f). Additionally, we observed the gradual decrease of the phase angle for high frequencies caused by the removal of water. Indeed, it is believed that the phase angle is related to the fractal dimension of the pore network within cement composites, with lower values indicating denser and more uniform microstructure.[44] Therefore, the evaporation of water from cement matrix pores may lead to the drop in phase angle curve. Similarly, it is highly visible that parameters of CPE_1 (Q-factor and α-exponent) are also partially related to the liquid ionic phase of cement mortars, since the progressive drying leads to the reduction of Q-factor and to the slight increase of α-exponent. Nevertheless, since DCPs are formed rather by small, closed pores and gel pores of C-S-H phase, the changes of saturation degree do not affect their electrical properties as much as in the case of CCPs.[44] Significantly, we find negligible difference in normalized C_1 capacitance for all drying conditions. Based on this result, we can confirm the nature of this parameter, being attributed to the solid fraction of cement paste layers independently on the moisture of cement composites.[40,45,46]

We then performed the impedance spectroscopy measurements of all mortars incorporating rGO after 5 days of oven-drying. Most importantly, our experimental results revealed a substantial change of the Nyquist plot shape (**Figures 5a-h**) with the increase of rGO loading. Such a unique behavior may point toward the formation of the conductive filler paths within cement matrix. Indeed, with the rGO addition exceeding 0.05 wt.%, the application of the equivalent circuit according to Figure 3a was no longer possible. Visibly, the experimental Nyquist plot indicates the presence of two semi-circles in the high frequency region as well as reveals significantly different ratio between the imaginary and real part of impedance. Moreover, to fully verify the effect of rGO on the electrical response of cement composites, we performed analogical measurements on mortars incorporating corresponding loadings of PCE (Figures S4a-e). Noteworthy, we noticed negligible difference in the shapes of Nyquist curves, with slight changes being most probably the fingerprint of increased porosity of samples prepared with the addition of superplasticizer.

This article is protected by copyright. All rights reserved.

15213765, ja, Downloaded from https://chemistry-europe.onlinelibrary.wiley.com/doi/10.1002/chem.202301816 by Cochrane France, Wiley Online Library on [13/10/2023]. See the Terms and Conditions (https://onlinelibrary.wiley.com/terms-and-conditions) on Wiley Online Library for rules of use; OA articles are governed by the applicable Creative Commons License

Accepted Manuscript

10.1002/chem.202301816

RESEARCH ARTICLE

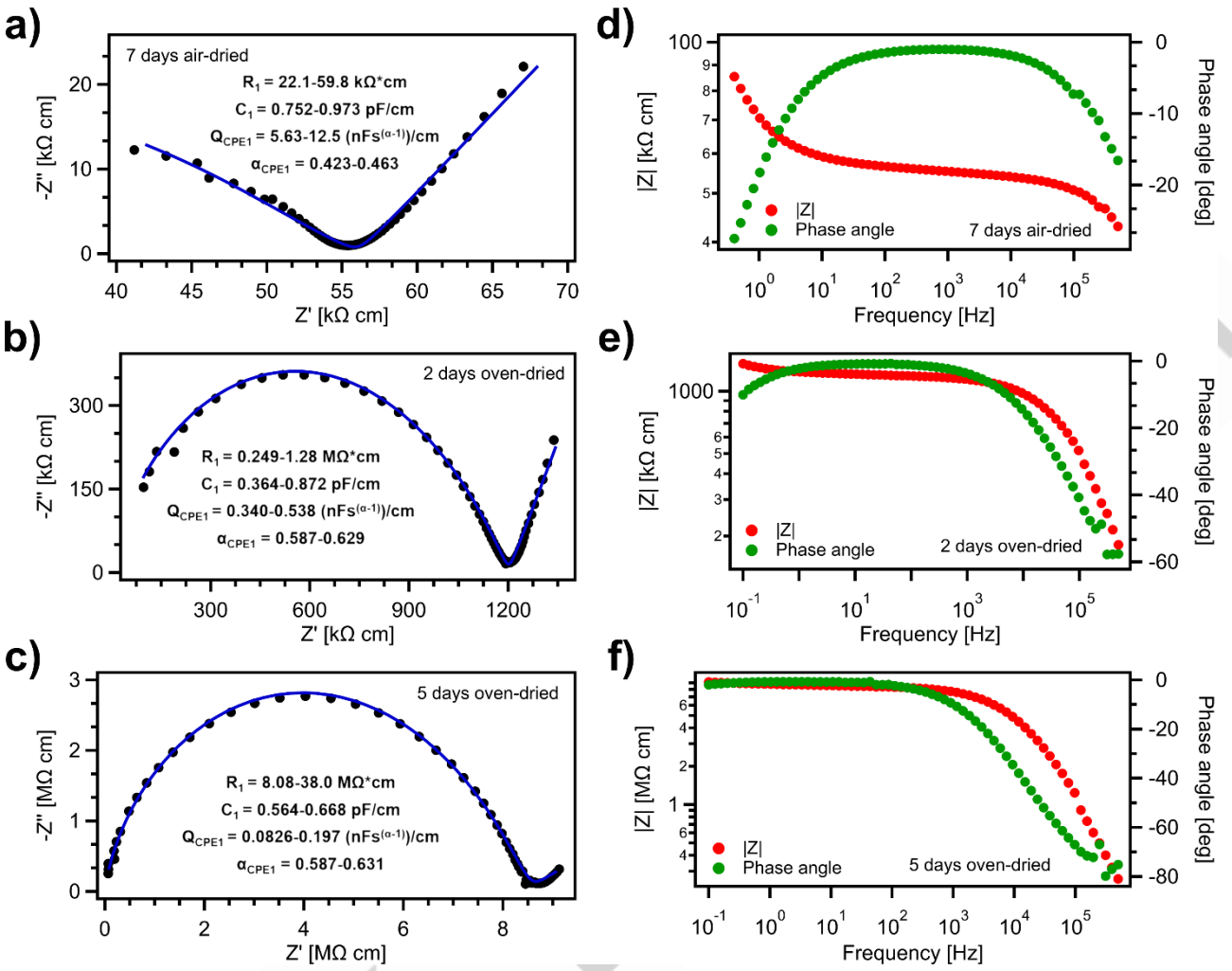

Figure 4. The results of EIS analysis of reference samples M1_R: a)-c) Nyquist plots with the values of equivalent circuit components and d)-f) Bode plots for a) and d) samples dried in the air for 7 days, b) and e) samples dried in the oven for 2 days and c) and f) samples dried in the oven for 5 days. Note: the values of the components of the equivalent circuit are normalized on the basis of the samples geometry and the distance between the electrodes.

This article is protected by copyright. All rights reserved.

15213765, ja, Downloaded from https://chemistry-europe.onlinelibrary.wiley.com/doi/10.1002/chem.202301816 by Cochrane France, Wiley Online Library on [13/10/2023]. See the Terms and Conditions (https://onlinelibrary.wiley.com/terms-and-conditions) on Wiley Online Library for rules of use; OA articles are governed by the applicable Creative Commons License

Accepted Manuscript

10.1002/chem.202301816

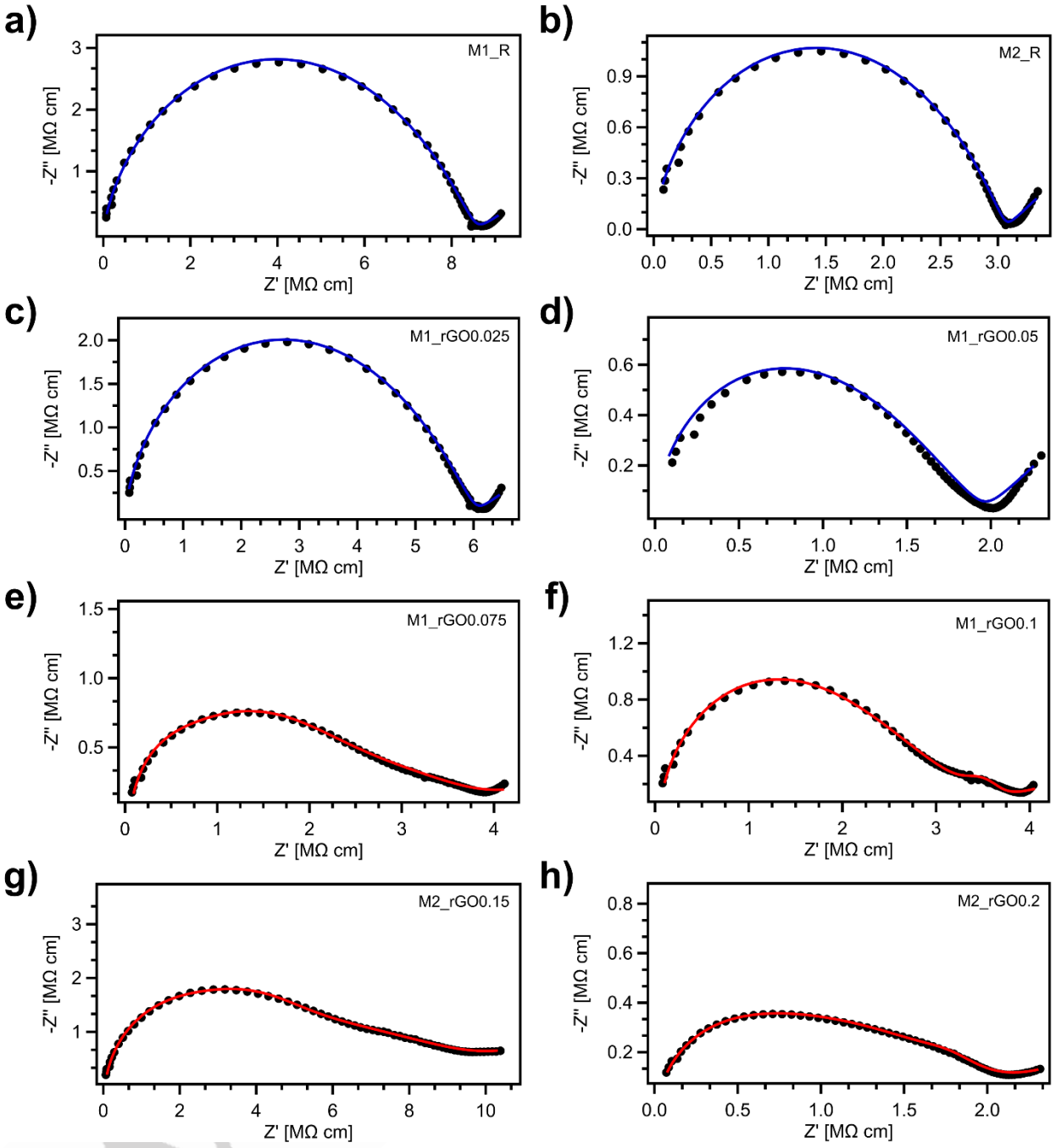

Figure 5. Nyquist plots for mortar samples dried in the oven for 5 days: a) and b) reference samples M1_R and M2_R, respectively, c)-h) samples containing rGO: M1_rGO0.025, M1_rGO0.05, M1_rGO0.075, M1_rGO0.1, M2_rGO0.15 and M2_rGO0.2. Note: blue colour represents the fitting with the equivalent electrical circuit according to Figure 3a, red colour – according to Figure 3b.

Therefore, we further modified the equivalent circuit for the rGO-based cement composites (see Figure 3b). Within this circuit, apart from the effects of the conductive paths of the bulk cement mortar and the electrode-specimen interface, we distinguished two additional rGO-based paths and introduced two new components: R_2 resistor and C_2 capacitor. While R_2 represents the impedance of continuous conductive paths of rGO flakes, C_2 simulates the capacitive behavior of solid cement paste layers between rGO flakes acting as capacitor plates. The total impedance value of the equivalent circuit presented in Figure 3b may be calculated as:

$$Z_B = \frac{1}{\frac{1}{R_1}+Q_1(j\omega)^{\alpha_1}+j\omega C_1} + \frac{1}{\frac{1}{R_2}+j\omega C_2} + \frac{1}{Q_e(j\omega)^{\alpha_e}} \quad (2)$$

Figure 6 displays the values of all components of the electrical equivalent circuits for reference cement mortars and rGO-based mortars after 5 days of oven drying. The corresponding values for PCE mortars may be found in Figure S5. Given that the increasing

This article is protected by copyright. All rights reserved.

15213765, ja, Downloaded from https://chemistry-europe.onlinelibrary.wiley.com/doi/10.1002/chem.202301816 by Cochrane France, Wiley Online Library on [13/10/2023]. See the Terms and Conditions (https://onlinelibrary.wiley.com/terms-and-conditions) on Wiley Online Library for rules of use; OA articles are governed by the applicable Creative Commons License

Accepted Manuscript

10.1002/chem.202301816

dosage of PCE is accompanied by a reduction of R_1 resistivity (Figure S5a) due to the higher porosity of the composites, we can conclude that low rGO additions do not influence the resistivity of continuous conductive paths in cement matrix (Figure 6a). Nevertheless, with high loading of rGO, *i.e.*, 0.15 wt.%, we observed a notable increase of the resistivity R_1, if compared with mortar M2_PCE0.15, from 0.57 MΩ cm to 7.90 MΩ cm. Even though rGO is electrically conductive, these results can be explained by the fact that rGO may partially participate in cement hydration, thus refining back the porosity of the composites. Noteworthy, the effect of rGO on the capacitance C_1 turned out to be marginal with the capacitance values of $6.3*10^{-13}$-$4.6*10^{-12}$ F cm^{-1}. Similarly, the slight increase recorded for samples with rGO addition above 0.075 wt.% can be ascribed to the refined microstructure of hardened mortars. Interestingly, rGO contributes to the notable increase of the Q-factor of CPE_1, simultaneously reducing the value of α-exponent (Figure 6c and d, Figure S5c and d). This is most probably due to two reasons: the modification of the pore network in cement matrix as well as the presence of randomly embedded rGO nanosheets along the discontinuous conductive paths of cement mortar.

Additionally, Figures 6a and b show the values of R_2 and C2 components of the rGO conductive paths created within cement matrix in mortars with rGO loading above 0.075 wt.%. The resistivity R_2 is associated with the resistivity of paths formed by rGO nanosheets placed close enough to each other to allow the tunneling conduction. Therefore, R_2 value drops with the increasing content of rGO due to the decreasing distance between the rGO nanosheets, achieving value of ca. 50 kΩ cm for mortar M2_rGO0.2. On the other hand, the capacitance C_2 represents the layers of cement matrix, where the number of rGO nanosheets is too low to allow the formation of conductive path, but instead leads to the formation of "rGO-cement-rGO capacitors". Therefore, the tremendous increase of the C_2 capacitance with high rGO dosage is associated as well with the decreasing distance between its nanosheets. Nevertheless, in this case one can expect that the capacitance C_2 will start to decrease again with higher rGO loadings allowing the contact conduction and therefore precluding further storage of electric charge.[27]

Noteworthy, most of the piezoresistive studies on self-sensing cement composites for potential applications in SHM conducted so far involved the resitivity-based measurements. For such measurements, the dosage of functional conductive filler needs to exceed the percolation threshold, since this method requires composites with at least medium resistivity, *i.e.*, ca. 10^3 Ω cm. Significantly, the use of impedance spectroscopy and the possibility to distinguish the conduction mechanisms of different paths within the composite may allow the self-sensing in composites with the loading of nanomaterials below the percolation threshold, due to the resistivity of functional filler paths or capacity-based sensing.[47]

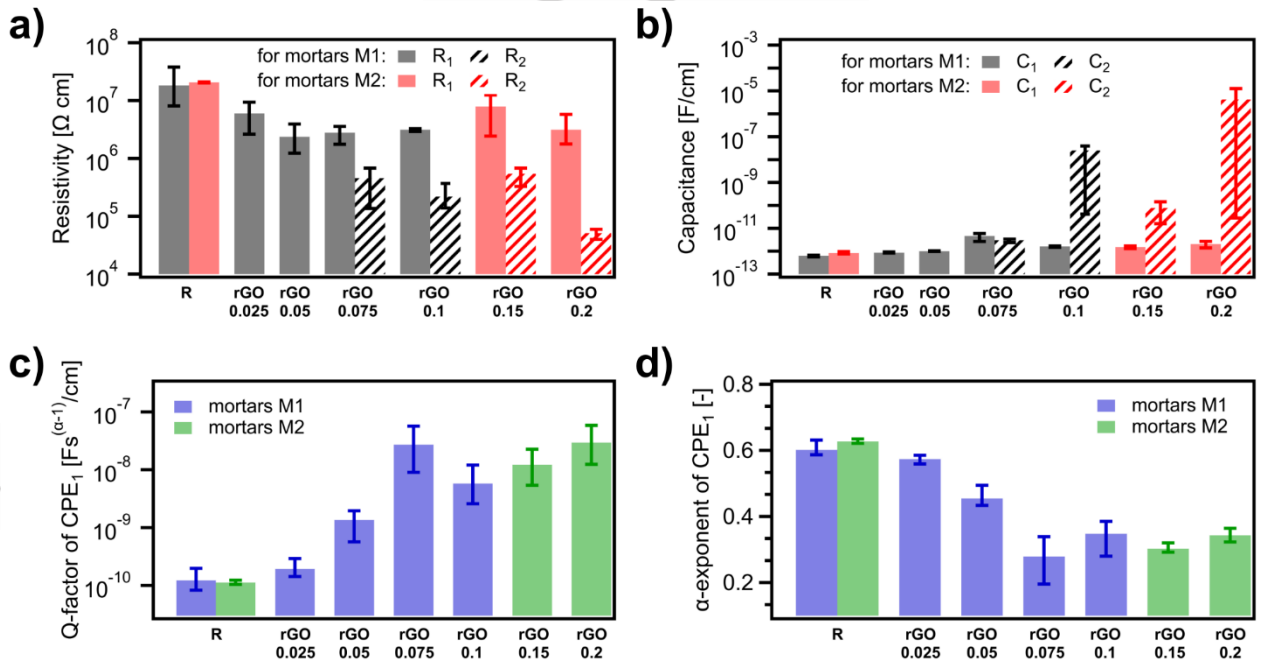

Figure 6. Values of the equivalent circuit components for reference cement mortars and mortars incorporating rGO, dried in the oven for 5 days: a) R1 and R2, b) C1 and C2, c) Q-factor and d) α-exponent of CPE1. Note: the values of the components of the equivalent circuit are normalized on the basis of the samples' geometry and the distance between the electrodes.

This article is protected by copyright. All rights reserved.

15213765, ja, Downloaded from https://chemistry-europe.onlinelibrary.wiley.com/doi/10.1002/chem.202301816 by Cochrane France, Wiley Online Library on [13/10/2023]. See the Terms and Conditions (https://onlinelibrary.wiley.com/terms-and-conditions) on Wiley Online Library for rules of use; OA articles are governed by the applicable Creative Commons License

Accepted Manuscript

10.1002/chem.202301816

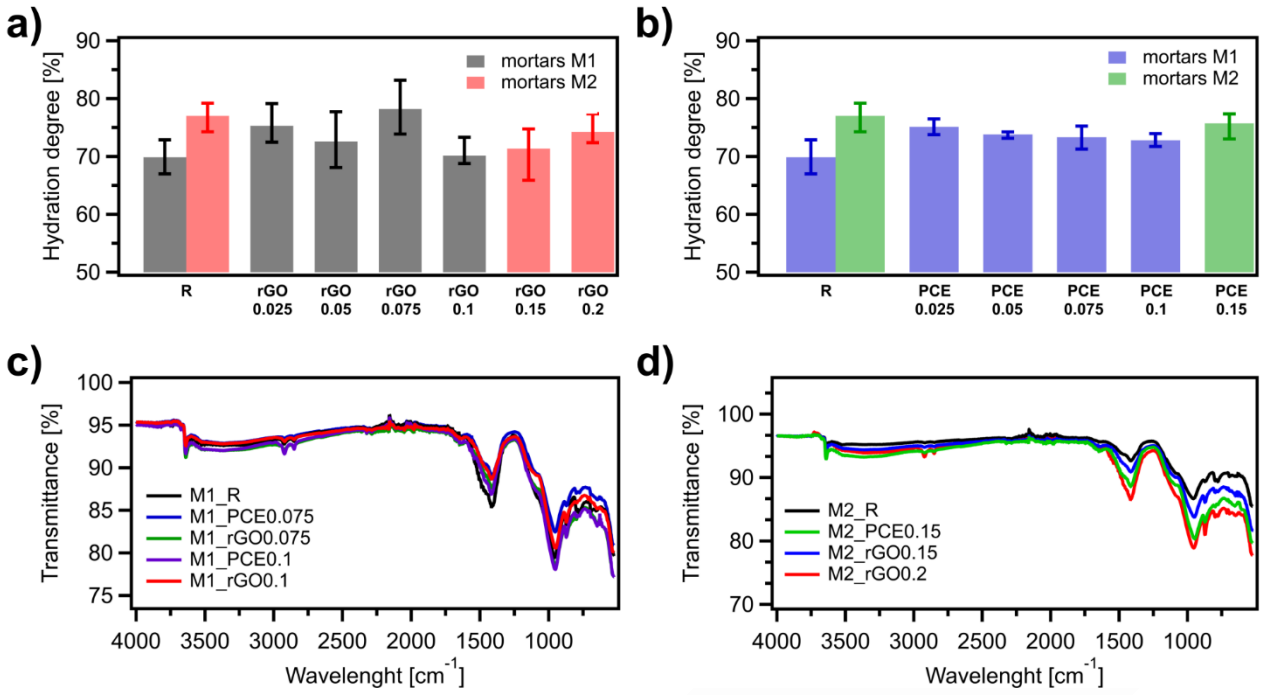

Figure 7. Structural characterization of cement mortars at the age of 28 days: a) and b) hydration degree of all mortars a) M1 and b) M2, c) and d) FTIR spectra of chosen mortars c) M1 and d) M2.

Microstructure and Composition

Since the high dosages of functional fillers required to obtain an appropriate electrical response may inhibit cement hydration and lead to the deteriorated microstructure of cement composites, we then decided to perform the structural characterization of all cement mortars at the age of 28 days by means of Thermogravimetric Analysis (TGA) and Fourier Transform Infrared Spectroscopy (FTIR).

Based on TGA measurements, we first calculated the hydration degree at the age of 28 days for all cement mortars (**Figures 7a** and **b**). We observed a slight increase of the hydration degree in all mortars containing PCE. In case of rGO-based cement mortars, rGO addition of 0.075 wt.% occurred as the most beneficial one, increasing the hydration degree from 69.9% and 73.4% obtained for reference mortar M1 and mortar M1_PCE0.075, respectively, up to 78.2%. For higher dosages of rGO, the hydration degree was comparable in both types of mortars: PCE and rGO/PCE. Nevertheless, in all cases the hydration degree was higher than in reference composites, hence even the highest loading of rGO does not hinder the cement hydration and the microstructure of the composites remains undeteriorated. The TGA results were further confirmed by FT-IR experiments (Figure 7c and d). Noteworthy, the intense band at 955 cm^{-1} indicates the stretching vibration of Si-O bonds of C-S-H phase revealing the highest formation of C-S-H gel in cement mortar reinforced with 0.075 wt.% and 0.2 wt.% of rGO for M1 and M2 composites, respectively.

Conclusion

In summary, we have demonstrated a novel cementitious nanocomposite incorporating reduced graphene oxide which features remarkably enhanced electrical properties. We first established simple and efficient method for obtaining homogeneous and stable rGO water dispersion, and thus for producing cement-graphene composites. The preparation method described involves the sonication of rGO with the addition of commercially available PCE superplasticizer with rGO-to-surfactant ratio of 1:2. We then applied electrochemical impedance spectroscopy to investigate the electrical properties of cement mortars incorporating rGO. The comprehensive EIS study conducted on reference mortars, mortars with PCE addition and rGO-based mortars at different drying conditions allowed us to propose a new, modified “conductive paths” model and electrical equivalent circuit giving a high compliance with experimental results. Within this model, we could distinguish conductive paths of bulk cement mortar as well as separate conductive paths formed by rGO nanosheets and cement layers, enabling the full interpretation of conduction mechanism of rGO-based cement composites. We observed the formation of additional rGO tunneling conduction paths with the rGO content as low as 0.075 wt.%. It should be highlighted that, to the best of our knowledge, the impedance spectroscopy has not been yet applied in the investigation of the electrical properties and conduction mechanism of rGO-based cement composites, therefore our observations open new possibilities for successful application of impedance spectroscopy in exploring the electrical behaviour of

This article is protected by copyright. All rights reserved.

15213765, ja, Downloaded from https://chemistry-europe.onlinelibrary.wiley.com/doi/10.1002/chem.202301816 by Cochrane France, Wiley Online Library on [13/10/2023]. See the Terms and Conditions (https://onlinelibrary.wiley.com/terms-and-conditions) on Wiley Online Library for rules of use; OA articles are governed by the applicable Creative Commons License

Accepted Manuscript

these composites. Overall, such findings provide unambiguous evidence that our composite can boost the practical application of graphene in SHM. The multifunctional cementitious composites incorporating rGO will allow the efficient monitoring of concrete structures thus extending their durability. Therefore, the reduced consumption of concrete components may contribute to the mitigation of the environmental issues related to concrete production.

Supporting Information

The authors have cited additional references within the Supporting Information.[28,33,47,49]

Acknowledgements

We are grateful to Abed El Kader Chamma for having performed first experiment on this project. We also acknowledge financial support from the Polish National Science Center (Grant No. 2019/33/NST5/00832), the European Commission through the Graphene Flagship Core 3 project (GA- 881603), as well as the Agence Nationale de la Recherche through the Interdisciplinary Thematic Institute SysChem via the IdEx Unistra (ANR-10-IDEX-0002) within the program Investissement d'Avenir program, the Foundation Jean-Marie Lehn, the Institut Universitaire de France (IUF) and the University of Strasbourg Institute for Advanced Study (USIAS).

Keywords: cement • conducting materials • electrical properties • impedance spectroscopy • graphene

[1] S. A. Miller, F. C. Moore, *Nat. Clim. Chang.* **2020**, *10*, 439–443.

[2] P. J. M. Monteiro, S. A. Miller, A. Horvath, *Nat. Mater.* **2017**, *16*, 698–699.

[3] A. M. Neville, *Properties of Concrete. 5th Edition.*, Pearson Education Limited, Harlow, England, **2011**.

[4] K. Barri, Q. Zhang, J. Kline, W. Lu, J. Luo, Z. Sun, B. E. Taylor, S. G. Sachs, L. Khazanovich, Z. L. Wang, A. H. Alavi, *Adv. Mater.* **2023**, *2211027*, 1–11.

[5] S. A. Miller, A. Horvath, P. J. M. Monteiro, *Nat. Sustain.* **2018**, *1*, 69–76.

[6] F. Wang, Y. Du, D. Jiao, J. Zhang, Y. Zhang, Z. Liu, Z. Zhang, *Adv. Sci.* **2021**, *8*, 1–11.

[7] T. Watari, Z. Cao, S. Hata, K. Nansai, *Nat. Commun.* **2022**, *13*, 1–9.

[8] G. Habert, S. A. Miller, V. M. John, J. L. Provis, A. Favier, A. Horvath, K. L. Scrivener, *Nat. Rev. Earth Environ.* **2020**, *1*, 559–573.

[9] M. Mishra, P. B. Lourenço, G. V. Ramana, *J. Build. Eng.* **2022**, *48*, 103954.

[10] S. Taheri, *Constr. Build. Mater.* **2019**, *204*, 492–509.

[11] Z. Tian, Y. Li, J. Zheng, S. Wang, *Compos. Part B Eng.* **2019**, *177*, 107437.

[12] M. J. Hanus, A. T. Harris, *Prog. Mater. Sci.* **2013**, *58*, 1056–1102.

[13] B. Han, X. Yu, J. Ou, in *Self-Sensing Concr. Smart Struct.*, Elsevier, **2014**, pp. 189–230.

[14] B. Han, X. Yu, J. Ou, B. Han, X. Yu, J. Ou, in *Self-Sensing Concr. Smart Struct.*, Elsevier, **2014**, pp. 163–187.

[15] B. Han, S. Ding, X. Yu, *Measurement* **2015**, *59*, 110–128.

[16] B. Han, X. Yu, J. Ou, B. Han, X. Yu, J. Ou, in *Self-Sensing Concr. Smart Struct.*, Elsevier, **2014**, pp. 13–43.

[17] K. S. Novoselov, A. K. Geim, S. V. Morozov, D. Jiang, Y. Zhang, S. V. Dubonos, I. V. Grigorieva, A. A. Firsov, *Science.* **2004**, *306*, 666–669.

[18] A. K. Geim, K. S. Novoselov, *Nat. Mater.* **2007**, *6*, 183–191.

[19] J. Kim, L. J. Cote, J. Huang, *Acc. Chem. Res.* **2012**, *45*, 1356–1364

[20] V. Singh, D. Joung, L. Zhai, S. Das, S. I. Khondaker, S. Seal, *Prog. Mater. Sci.* **2011**, *56*, 1178–1271.

[21] R. Raccichini, A. Varzi, S. Passerini, B. Scrosati, *Nat. Mater.* **2015**, *14*, 271–279.

[22] H. Shin, K. K. Kim, A. Benayad, S. Yoon, H. K. Park, I. Jung, M. H. Jin, H. Jeong, J. M. Kim, J. Choi, Y. H. Lee, *Adv. Funct. Mater.* **2009**, *19*, 1987–1992.

[23] C. Valentini, V. Montes-García, P. A. Livio, T. Chudziak, J. Raya, A. Ciesielski, P. Samorì, *Nanoscale* **2023**, *15*, 5743–5755.

[24] H. C. Schniepp, J. Li, M. J. McAllister, H. Sai, M. Herrera-Alonso, D. H. Adamson, R. K. Prud'homme, R. Car, D. A. Saville, I. A. Aksay, *J. Phys. Chem. B* **2006**, *110*, 8535–8539.

[25] B. Han, X. Yu, J. Ou, B. Han, X. Yu, J. Ou, in *Self-Sensing Concr. Smart Struct.*, Elsevier, **2014**, pp. 67–93.

[26] X. Hu, C. Shi, X. Liu, J. Zhang, G. de Schutter, *Cem. Concr. Compos.* **2019**, *100*, 1–14.

[27] W. Pichór, M. Frąc, M. Radecka, *Cem. Concr. Compos.* **2022**, *125*, 104328.

[28] H. Wang, A. Zhang, L. Zhang, Q. Wang, X. Yang, X. Gao, F. Shi, *Constr. Build. Mater.* **2020**, *265*, 120740.

[29] N. Karim, S. Afroj, S. Tan, P. He, A. Fernando, C. Carr, K. S. Novoselov, *ACS Nano* **2017**, *11*, 12266–12275.

[30] Y. Lin, H. Du, *Constr. Build. Mater.* **2020**, *265*, 120312.

[31] H. Yang, M. Monasterio, H. Cui, N. Han, *Compos. Part A Appl. Sci. Manuf.* **2017**, *102*, 263–272.

[32] X. Li, A. H. Korayem, C. Li, Y. Liu, H. He, J. G. Sanjayan, W. H. Duan, *Constr. Build. Mater.* **2016**, *123*, 327–335.

[33] G. Jing, Z. Ye, J. Wu, S. Wang, X. Cheng, V. Strokova, V. Nelyubova, *Cem. Concr. Compos.* **2020**, *109*, 103559.

[34] M. Safuta, A. Ciesielski, P. Samorì, in *Concr. Innov. Sustain. Proc. 6th Fib Int. Congr.* (Eds.: S. Stine, B. Henny), Novus Press, Oslo, Norway, **2021**.

[35] T. S. Qureshi, D. K. Panesar, *Constr. Build. Mater.* **2019**, *206*, 71–83.

[36] M. Murugan, M. Santhanam, S. Sen Gupta, T. Pradeep, S. P. Shah, *Cem. Concr. Compos.* **2016**, *70*, 48–59.

[37] S. Sun, B. Han, S. Jiang, X. Yu, Y. Wang, H. Li, J. Ou, *Constr. Build. Mater.* **2017**, *136*, 314–328.

[38] Y. Zhao, Y. Liu, T. Shi, Y. Gu, B. Zheng, K. Zhang, J. Xu, Y. Fu, S. Shi, *Constr. Build. Mater.* **2020**, *257*, 119498.

[39] Y. Kim, J. Lee, S. Hong, *Cem. Concr. Res.* **2003**, *33*, 299–304.

[40] M. Cabeza, P. Merino, A. Miranda, X. R. Nóvoa, I. Sanchez, *Cem. Concr. Res.* **2002**, *32*, 881–891.

[41] F. He, R. Wang, C. Shi, R. Zhang, C. Chen, L. Lin, X. An, *Constr. Build. Mater.* **2017**, *143*, 179–188.

[42] G. Song, *Cem. Concr. Res.* **2000**, *30*, 1723–1730.

[43] J. M. Cruz, I. C. Fita, L. Soriano, J. Payá, M. V. Borrachero, *Cem. Concr. Res.* **2013**, *50*, 51–61.

[44] T. Shi, L. Zheng, X. Xu, *Constr. Build. Mater.* **2017**, *145*, 548–554.

[45] I. S. C. Antón, G. D. V. J. M. Ortega, M. A. Climent, **2013**, 362–371.

This article is protected by copyright. All rights reserved.

15213765, ja, Downloaded from https://chemistry-europe.onlinelibrary.wiley.com/doi/10.1002/chem.202301816 by Cochrane France, Wiley Online Library on [13/10/2023]. See the Terms and Conditions (https://onlinelibrary.wiley.com/terms-and-conditions) on Wiley Online Library for rules of use; OA articles are governed by the applicable Creative Commons License

Accepted Manuscript

10.1002/chem.202301816

[46] H. Sun, Z. Ren, S. Ali, D. Zhao, X. Zhang, D. Li, *Constr. Build. Mater.* **2017**, *135*, 361–368.

[47] D. D. L. Chung, *Sensors Actuators A Phys.* **2023**, *354*, 114270.

[48] S. M. Monteagudo, A. Moragues, J. C. Gálvez, M. J. Casati, E. Reyes, *Thermochim. Acta* **2014**, *592*, 37–51.

[49] Graphenea “Graphene Oxide Product Datasheet”, can be found under https://www.graphenea.com/collections/graphene-oxide/products/graphene-oxide-4-mg-ml-water-dispersion-1000-ml (accessed 13 September 2023)

This article is protected by copyright. All rights reserved.

15213765, ja, Downloaded from https://chemistry-europe.onlinelibrary.wiley.com/doi/10.1002/chem.202301816 by Cochrane France, Wiley Online Library on [13/10/2023]. See the Terms and Conditions (https://onlinelibrary.wiley.com/terms-and-conditions) on Wiley Online Library for rules of use; OA articles are governed by the applicable Creative Commons License

Accepted Manuscript

10.1002/chem.202301816

WILEY VCH

RESEARCH ARTICLE

Entry for the Table of Contents

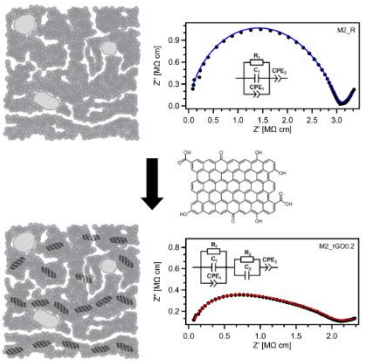

Multifunctional rGO-based cement composite featuring remarkably enhanced electrical properties was developed. Simple and efficient method for obtaining homogeneous and stable rGO dispersion in cement composites was established. Electrochemical impedance spectroscopy was applied to investigate the conduction mechanisms within rGO-based cement mortar and new electrical equivalent circuit was proposed.

Institute and/or researcher Twitter usernames:

This article is protected by copyright. All rights reserved.

15213765, ja, Downloaded from https://chemistry-europe.onlinelibrary.wiley.com/doi/10.1002/chem.202301816 by Cochrane France, Wiley Online Library on [13/10/2023]. See the Terms and Conditions (https://onlinelibrary.wiley.com/terms-and-conditions) on Wiley Online Library for rules of use; OA articles are governed by the applicable Creative Commons License